Hydration repulsion between biomembranes results from an interplay of dehydration and depolarization

Emanuel Schneck[a,b,1], Felix Sedlmeier[a,b], and Roland R. Netz[a,b]

[a]Fachbereich Physik, Freie Universität Berlin, Arnimallee 14, 14195 Berlin, Germany; and [b]Physik Department, Technische Universität München, 85748 Garching, Germany

Edited by B. J. Berne, Columbia University, New York, NY, and approved July 30, 2012 (received for review April 7, 2012)

Hydration repulsion dominates the interaction between polar surfaces in water at nanometer separations and ultimately prevents the sticking together of biological matter. Although confirmed by a multitude of experimental methods for various systems, its mechanism remained unclear. A simulation technique is introduced that yields accurate pressures between solvated surfaces at prescribed water chemical potential and is applied to a stack of phospholipid bilayers. Experimental pressure data are quantitatively reproduced and the simulations unveil a rich microscopic picture: Direct membrane–membrane interactions are attractive but overwhelmed by repulsive indirect water contributions. Below about 17 water molecules per lipid, this indirect repulsion is of an energetic nature and due to desorption of hydration water; for larger hydration it is entropic and suggested to involve water depolarization. This antagonistic nature and the presence of various compensating contributions indicate that the hydration repulsion is less universal than previously assumed and rather involves finely tuned surface-water interactions.

solvation | MD simulation | phospholipids

Hydration repulsion (HR) universally acts between well-solvated surfaces in water and balances the van der Waals attraction in the nanometer range. It ultimately prevents the collapse of biological matter and thereby provides macromolecular assemblies with the necessary lubrication for vital functioning, even in the congested cell environment. Although complex in its nature, it is rightfully considered a fundamental force in solution chemistry and structural biology (1). HR was first quantified experimentally for stacks of charge-neutral phospholipid bilayer membranes in terms of pressure–distance curves (2–4), confirmed for two individual bilayers by the surface force apparatus (SFA) (5, 6), and is now known to universally act between nucleic acids, proteins, and polysaccharides alike (7). It exhibits an exponential decay with a decay length of a few Ångstrom (4) and as a heuristic law is nowadays commonly used in modeling the forces between polar surfaces in water (8). Although several theoretical (9–11) and simulation (12–18) studies elucidated partial aspects of the HR, none treated the full complexity of the problem and could quantitatively reproduce and explain experimental pressure–distance curves, meaning that the HR mechanism remained essentially unclear. The reason for this is obvious: Theory typically only treats one part of the problem, be it the water–water interactions, the water–surface binding, or the configurational entropy of bilayer molecules, whereas current simulation strategies account for the constant water chemical potential either in the form of a large reservoir (13–15) or by grand-canonical simulations (16, 17). Due to limitations in the numerical accuracy, however, both approaches do not enable quantitative comparison of the HR pressure with experimental data. We solve this problem by introducing the thermodynamic extrapolation method (TEM), which allows performing bilayer simulations in the constant water number ensemble at a prescribed water chemical potential, without the need for time-consuming water insertion/deletion steps or an embedding water reservoir (19). The pressure resolution is about $\Delta\Pi \approx 15$ atm, roughly the HR at 20 water molecules per lipid, thus allowing quantitative comparison with experiments in a wide range of hydration. This in turn allows us to unveil the HR mechanism by a detailed thermodynamic analysis of the various microscopic contributions.

Results and Discussion

Fig. 1*A* shows a simulation snapshot of $N_l = 72$ zwitterionic dipalmitoylphosphatidylcholine (DPPC) molecules hydrated by $N_w = 28 \times 72 = 2016$ extended simple point charge (SPC/E) water molecules that form a stable fluid bilayer without any positional restraints (20). We use the GROMACS simulation package (21) and a dedicated lipid force field (22), choose a fixed area per lipid of $A_l = 2A/N_l = 0.65$ nm^2, realistic for the fluid L_α-phase, and vary $n_w = N_w/N_l$ from 4 to 28 water molecules per lipid. The membrane and water density profiles (Fig. 1*B*) are in good agreement with experiments on fluid phospholipid membranes (23). Fig. 1*C* shows the simulated pressure–distance curve, $\Pi(D_w)$, in a semilogarithmic plot (black symbols), compared with experimental results for fluid lecithin multilayers at room temperature (red circles) (2), fluid DPPC multilayers at $T = 323$ K (blue squares) (4), and a single pair of lecithin bilayers using SFA (green triangles) (6). In analogy to experiments (3), we compute the water layer thickness D_w from the pressure-dependent molecular water volume v_w via $D_w = 2v_w n_w/A_l$. This first comparison between simulation and experimental hydration pressures is nearly quantitative in terms of the absolute pressure scale, the exponential decay length, and the shape of the $\Pi(D_w)$ curve, showing in particular the characteristic upturn at the smallest bilayer separations. This is even more compelling considering that in the experimental curves different bilayer compositions (DPPC versus lecithin, the latter consisting of phosphatidylcholine (PC) headgroups but polydisperse fatty acids), slightly different temperatures and different ensembles are used [multilayer experiments apply either isotropic hydrostatic or equivalent osmotic pressures (2, 4), whereas in the SFA and our simulations the lateral area per lipid is fixed (6)]. This good agreement between simulations and experiments we interpret as validation of our force fields and simulation methods, which therefore puts us in a position to analyze the simulations in more detail with the idea to unravel the mechanism behind the measured hydration repulsion. The main question we address with our simulations in essence is: What is it that keeps the bilayers separated even at high pressures of 10^8 Pa or 1,000 atm? To make progress in this direction, the pressure $\Pi = \Pi_{\mathrm{dir}} + \Pi_{\mathrm{ind}}$ is first decomposed into the direct membrane–membrane contribution and all other water-mediated forces, in the following denoted as the indirect contribution (13, 17). Note that this decomposition is indepen-

Author contributions: E.S. and R.R.N. designed research; E.S. and F.S. performed research; E.S. and F.S. analyzed data; and E.S. and R.R.N. wrote the paper.

The authors declare no conflict of interest.

This article is a PNAS Direct Submission.

Freely available online through the PNAS open access option.

[1]To whom correspondence should be addressed. E-mail: emanuel.schneck@tum.de.

This article contains supporting information online at www.pnas.org/lookup/suppl/doi:10.1073/pnas.1205811109/-/DCSupplemental.

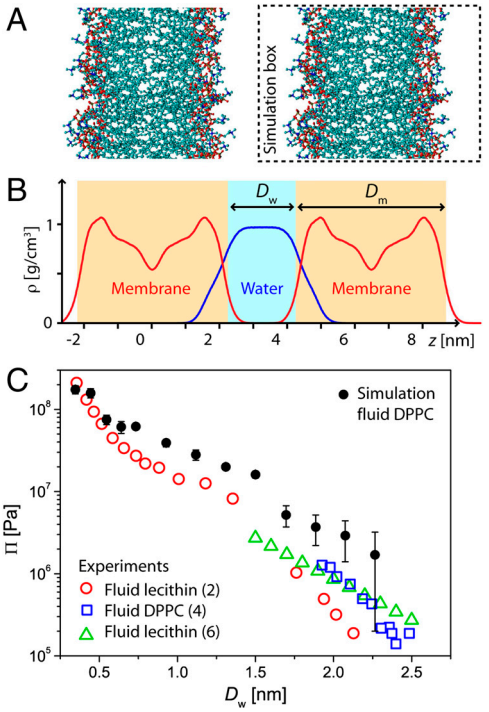

Fig. 1. Atomistic computer model of interacting phospholipid membranes and resulting interaction pressure. (*A*) Snapshot of the phospholipid bilayer in the fluid L_α-phase. The membrane is hydrated with 28 water molecules per lipid, $n_w = 28$. (*B*) Membrane and water density profiles along the surface normal. (*C*) Comparison of the interaction pressure Π from MD simulations (filled black symbols) with experimental results for lecithin multilayers (red circles) (2), DPPC multilayers (blue squares) (4), and a single pair of lecithin bilayers (green triangles, obtained from an exponential fit to the experimental free energy data and subsequent differentiation with respect to D_w) (6), all as a function of water layer thickness D_w. Error bars represent the standard error of the computed interaction pressures.

dent of the position of the surface through which the pressure is calculated as long as it lies entirely inside the water phase. In Fig. 2*A* one sees that $\Pi_{\rm dir}$ is strongly attractive, whereas $\Pi_{\rm ind}$ is repulsive and overcompensates the direct attraction throughout the studied hydration range. Such a near-cancellation is known from simple continuum models of van der Waals interactions between hydrocarbon assemblies in water and is also typical for charge interactions in aqueous solution due to dielectric effects (24); it has been seen in previous simulation studies at low hydration (17) and immediately rules out the direct interaction between bare lipid headgroups (be it steric or electrostatic) as an explanation for the hydration repulsion.

Although not at the heart of HR, a close look at the attractive direct interaction is revealing. To this end, the direct free energy, $G_{\rm dir} = H_{\rm dir} - TS_{\rm dir}$, is first calculated from $\Pi_{\rm dir}$ via integration and then decomposed into its enthalpic, $H_{\rm dir}$, and entropic, $-TS_{\rm dir}$, contributions as described in the *SI Text*. As seen in Fig. 2*B*, $G_{\rm dir}$ is dominated by the attractive enthalpic part $H_{\rm dir}$, whereas the entropy is repulsive. As shown in the *Inset* of Fig. 2*B*, $H_{\rm dir}$ is itself dominated by its electrostatic Coulombic part, with only a small Lennard–Jones (LJ) contribution. This Coulombic attraction is at first sight surprising because the PC headgroup dipoles point against each other, which might be thought to produce an unfavorable dipole–dipole interaction. In fact, orientational correlations between point dipoles have been previously argued to give rise to an attractive membrane–membrane interaction contribution (25). To gain microscopic insight into this, Fig. 2*D* shows the normalized radial distribution functions (rdfs) between the partially negatively charged phosphorus (P) and positive nitrogen (N) atoms in two opposing PC monolayers at high, $n_w = 20$ (dashed lines), and low, $n_w = 4$ (solid lines), hydration. For large surface separations $n_w = 20$, the rdfs are rather unstructured and reflect the unperturbed headgroup structure with N being displaced towards the water with respect to P. As a result, the N-N distribution is shifted to smaller distances compared to P-P, with N-P being intermediate. For small surface separation $n_w = 4$, the picture is drastically different. Now, the N-P distribution is peaked at a distance significantly shorter than the distributions N-N and P-P between like-charged groups. The schematic illustration in Fig. 2*E* highlights the lipid headgroup configurational reorganization at short separations, which minimizes the electrostatic energy. This reorganization, in turn, is accompanied by structural ordering and thus by a configurational entropy loss, as witnessed by the pronounced rdf peaks for $n_w = 4$, and can be considered the main origin for the entropic repulsion $-TS_{\rm dir}$ in Fig. 2*B*. This finding is conceptually related to the "protrusion model" for the hydration repulsion introduced by Israelachvili and Wennerström, which attributes the HR to a suppression of lipid protrusion modes at small distances (10). These results demonstrate that repulsion originating from the reduction in the configurational entropy of the membranes indeed contributes significantly to their interaction at small membrane separations. However, the configurational restriction on lipid headgroups is in the simulations not caused by steric repulsion (i.e., lipid heads colliding with each other) but rather is a by-product of the dominating electrostatic attraction between headgroups in opposing bilayers.

We now turn to the indirect water-mediated interaction and perform a similar decomposition, $G_{\rm ind} = H_{\rm ind} - TS_{\rm ind}$, into enthalpic and entropic parts. As expected based on the near-cancellation of direct and indirect pressure contributions in Fig. 2*A*, the behavior here is opposite to the direct pressure and the repulsive enthalpy $H_{\rm ind}$ dominates over the attractive entropy contribution $-TS_{\rm ind}$ for almost the entire distance range, as shown in Fig. 2*C*. Closer inspection at large separation, in the *Inset*, reveals that for $n_w > 17$ a reversal takes place and $H_{\rm ind}$ is attractive whereas $-TS_{\rm ind}$ is repulsive. Again, microscopic insight can be gathered from simulation data, this time from the interfacial water density profiles $\rho(z)$ in Fig. 3*A*: As the bilayers approach each other and water is removed from the system, $\rho(z)$ stays invariant up to the water slab center, apart from a small shift Δz accounting for membrane compression. The hydration level $n_w = 16$ demarks a crossover. For larger hydration the removed water is bulk-like; for smaller hydration the removed water deviates from bulk behavior and is of distinct interfacial nature. This picture is corroborated by profiles $h_{\rm ind}(z)$ for the excess enthalpy per water molecule in Fig. 3*B*, which is related to the indirect enthalpy via an integral over the whole water density distribution,

$$H_{\rm ind} = \int {\rm d}z h_{\rm ind}(z)\rho(z)/m_w,$$

with m_w the mass of a water molecule: Water is enthalpically strongly bound to the bilayers (vice versa, because the chemical potential of water is constant, there is an equally strong entropic repulsion). In the low-hydration state, exemplified by the curve for $n_w = 8$, water right in the slab middle (denoted by a vertical broken line) is more strongly bound compared to the high-hydration case ($n_w = 28$) at the same separation from the bilayer (this difference is highlighted by the blue area), but this amplification of binding is more than compensated by the removal of strongly bound interfacial water (highlighted by the orange area). The net effect is the strong enthalpic indirect repulsion seen in Fig. 2*C*. We note that this interfacial water binding, although mostly of electrostatic origin (as shown in the *SI Text*), points to pronounced deviations from bulk water dielectric behavior, for which electrostatic binding is known to be of entropic nature (24). This

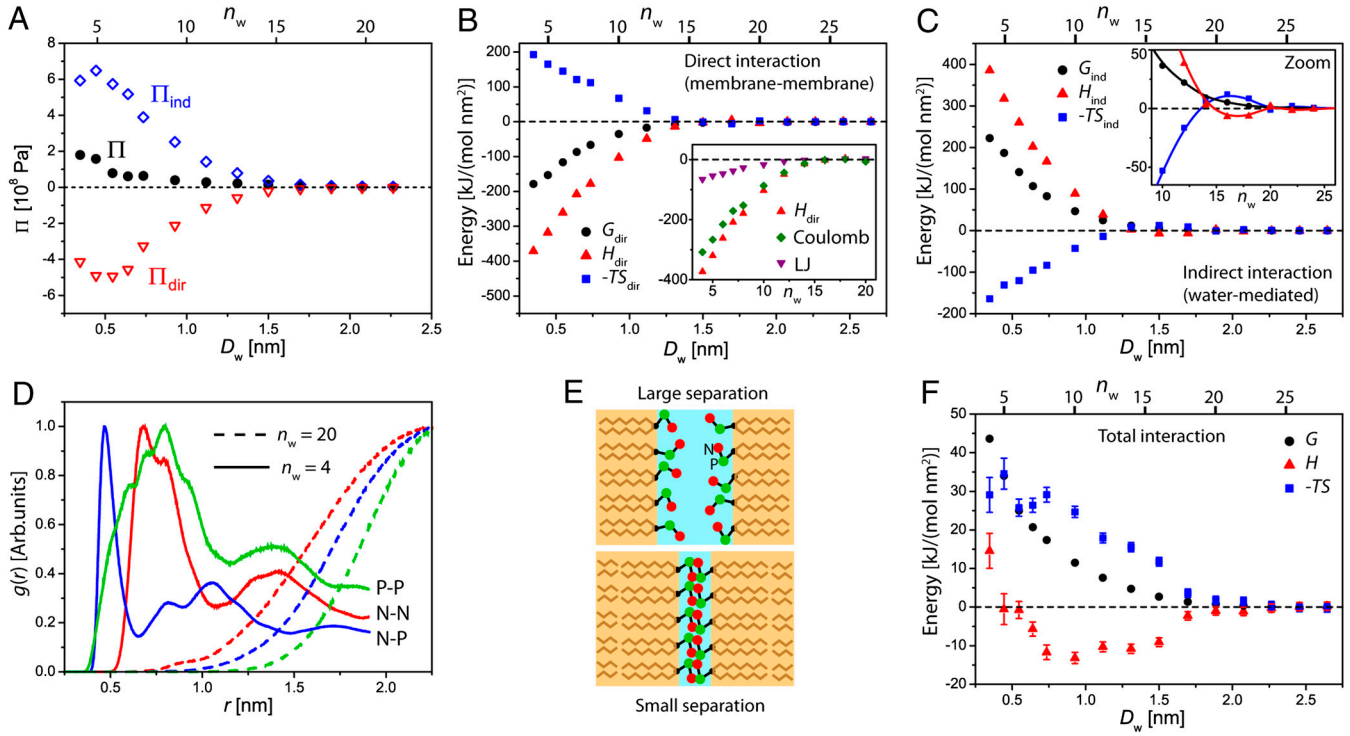

Fig. 2. Decomposition into direct and water-mediated indirect interactions. (*A*) Total pressure $\Pi = \Pi_{dir} + \Pi_{ind}$ and its direct (Π_{dir}) and indirect (Π_{ind}) contributions versus D_w (lower axis) and n_w (upper axis). (*B*) Free energy G_{dir} of the direct membrane–membrane interaction and its enthalpic (H_{dir}) and entropic ($-TS_{dir}$) parts. *Inset*: Coulomb and LJ contributions to H_{dir}. (*C*) Free energy G_{ind} of the indirect, water-mediated interaction and its enthalpic (H_{ind}) and entropic ($-TS_{ind}$) parts. The *Inset* shows a close-up view for high hydration (solid lines serve as guides to the eye). (*D*) Normalized radial distribution functions $g(r)$ between nitrogen (N) and phosphate (P) atoms in the opposing PC headgroup regions at high (dashed lines) and low (solid lines) hydration. (*E*) Schematic illustration of the headgroup reorganization upon dehydration. (*F*) Free energy *G* of the total interaction and its enthalpic (*H*) and entropic (*−TS*) parts. Error bars represent the standard error of the computed thermodynamic quantities.

is in line with recent simulations pointing to strong deviations of the interfacial water dielectric response from bulk behavior (26).

But is this liberation of enthalpically bound water from the hydration layers, i.e., the forced dehydration of the PC headgroup region, the whole story or are there effects that have to do with water polarization and interactions between such polarized water layers, as assumed in the early theoretical treatments (9, 11)? Symbols in Fig. 3*C* show water polarization profiles at high ($n_w = 28$) and intermediate ($n_w = 16$) hydration in terms of the mean water dipole angle projected on the bilayer normal, $\langle \cos\theta \rangle$. Close to the membrane surface, water dipoles are strongly oriented, whereas in the water slab center the polarization by symmetry vanishes, as depicted schematically in Fig. 3*D*. As the hydration decreases, the polarization profiles from the two opposing surfaces interfere destructively, resulting in pronounced depolarization, indicated by the gray area in Fig. 3*C*. The solid lines in Fig. 3*C* are predictions from Marcelja's theory for the hydration repulsion between bilayers, based on a general free energy expansion in terms of an unspecified orientational order parameter (11) (see *SI Text*). The good agreement with our data suggests that water polarization effects are indeed operative at large distances and can be described by Marcelja's general ideas, but additional effects that involve nonlocal effects and quadrupolar or other order parameters are likely to play an important role as well (26). The crossover of the indirect repulsion from being enthalpic, for $n_w < 17$ to being entropic, for $n_w > 17$, finally points to a change of the dielectric behavior from interface-dominated to bulk-like at about a separation of 1 nm from the bilayer surface, in full accord with simulation results for interfacial dielectric profiles (26).

Although the total free energy *G* in Fig. 2*F* is monotonically increasing with decreasing hydration, the total enthalpy $H = H_{dir} + H_{ind}$ displays a minimum at a hydration of about $n_w = 9$. Such a crossover between enthalpic attraction and repulsion has been experimentally observed (27, 28) for gel-phase DPPC bilayers at about $n_w = 4$–5. Based on our findings, this crossover arises from the competition between enthalpic direct attraction in Fig. 2*B* and enthalpic indirect repulsion in Fig. 2*C* and demonstrates the intricate interplay of hydration and membrane–membrane interaction effects. Previous simulation studies where bilayer head groups were firmly arranged on lattices did not exhibit the entropic repulsion regime (14), which suggests that the conformational freedom of lipids plays a crucial role. Although the quantitative agreement between experimental and our simulated pressure curves for PC-lipids in Fig. 1*C* lends credibility to our simulation results, this enthalpy crossover constitutes an independent validation of the current modeling and in particular the crossover between direct (membrane–membrane) and indirect (water-mediated) interaction effects.

Conclusions

The grand picture that emerges from our simulations is the following: For large bilayer separations, each membrane has an intact and strongly bound hydration layer, and the repulsion can be associated with the destructive interaction between the water polarization layers (11); in this distance regime we thus suggest the interbilayer pressure profile to be universal, however, with a dependence on the boundary condition imposed by the headgroup-induced water ordering (9). Based on Marcelja's theory, the repulsion in this asymptotic distance range decays exponentially, in agreement with our numerical findings. For smaller degrees of hydration, the hydration layers overlap, and strongly bound water is removed; at the same time, direct membrane–membrane interactions start to kick in. In this distance regime, the pressure involves the subtle interplay of headgroup interactions between the opposing bilayer surfaces and the way water is

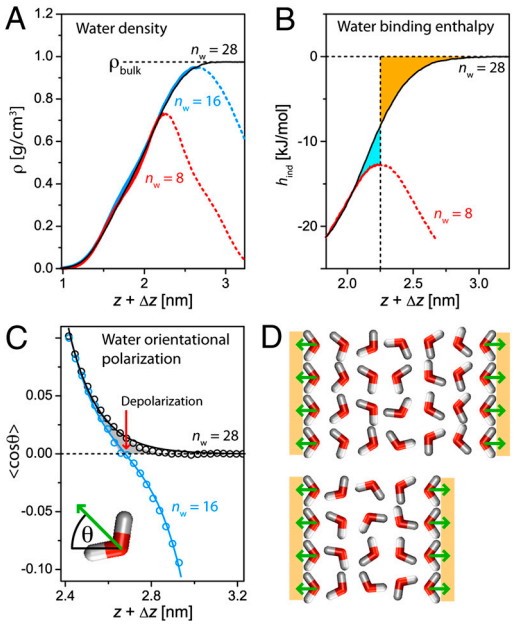

Fig. 3. Mechanisms of the water-mediated repulsion. (*A*) Water density profiles $\rho(z)$ between membrane surfaces for different hydration degrees ($n_w = 28$ and $\Delta z = 0$, $n_w = 16$ and $\Delta z = 0.023$ nm, and $n_w = 8$ and $\Delta z = 0.066$ nm). (*B*) Profiles of enthalpy per water molecule $h_{\mathrm{ind}}(z)$ at high ($n_w = 28$) and low ($n_w = 8$) hydration. (*C*) Simulated water dipole orientation profiles $\langle \cos\theta \rangle$ (symbols) at high ($n_w = 28$) and intermediate ($n_w = 16$) hydration. The gray area denotes the depolarization effect. Solid lines are fits according to Marcelja's general theory for hydration repulsion in terms of a scalar orientational order parameter profile (11). (*D*) Schematic illustration of interfacial water orientation at high (*Upper*) and small (*Lower*) bilayer separation.

incorporated into the headgroup region; we therefore expect less universal behavior that depends in the first place on headgroup chemistry and to a lesser degree also on the lipid chain length. The pressure in this distance range is in general not following an exponential law. In essence, what we are faced with are antagonistic effects on various levels: a competition between direct membrane–membrane and indirect water-mediated interactions, crossovers between entropic and enthalpic contributions, and a shift from a dehydration to a depolarization mechanism of the indirect repulsion as hydration goes up. Note that undulation forces due to the restriction of large-scale membrane shape fluctuations (29) are unimportant for the rather stiff bilayers and in the distance range we have considered, which is confirmed by the good agreement in Fig. 1*C* between experimental results for freely undulating membrane stacks and the SFA data where bilayers are bound to solid supports. Finally, a look at numbers is revealing: Whereas the direct free energy in Fig. 2*B* at the smallest hydration $n_w = 4$ is attractive and $G_{\mathrm{dir}} = -180\ \mathrm{kJ/(mol\,nm^2)}$, the indirect free energy in Fig. 2*C* at $n_w = 4$ is repulsive and $G_{\mathrm{ind}} = 225\ \mathrm{kJ/(mol\,nm^2)}$, giving a repulsive total free energy of $G = 45\ \mathrm{kJ/(mol\,nm^2)}$: Massive cancellation takes place. Therefore, small experimental modifications or simulation inaccuracies in either direct or indirect contributions can give rise to large net effects, making the simulation of such systems challenging in terms of developing reliable force fields and efficient simulation methods; our thermodynamic extrapolation method is a step in that direction.

Methods

The Thermodynamic Extrapolation Method. The interaction pressure Π between two surfaces at a certain surface separation (i.e., water layer thickness) D_w follows from the Gibbs free energy per area, G, as

$$\Pi(D_w) = -\left(\frac{dG}{dD_w}\right)_{\mu_0}, \qquad [1]$$

where the number of water molecules N_w between the surfaces is not fixed but controlled by the bulk chemical potential μ_0. Our TEM involves two distinct sets of simulations, the first performed in the (N_w, D) ensemble where N_w water molecules are placed between two phospholipid bilayer surfaces at fixed box height $D = D_m + D_w$, where D_m denotes the membrane thickness as indicated in Fig. 1*B*. All simulations are performed at constant lateral area A and temperature $T = 320$ K. The actual water chemical potential μ, which in general deviates substantially from the bulk value μ_0, together with the pressure $\Pi_{\mu\neq\mu_0}(N_w)$, which consequently also differs from the desired pressure $\Pi(N_w)$, are determined with high precision. Using the formally exact thermodynamic relation, $\Pi(N_w) = \Pi_{\mu\neq\mu_0}(N_w) - \Delta\Pi(N_w, \mu_0, \mu)$, the pressure at μ_0 can be approximated to first order in the deviation $\mu - \mu_0$ as

$$\Pi(N_w) \approx \Pi_{\mu\neq\mu_0}(N_w) - \frac{\mu - \mu_0}{v_w^0}, \qquad [2]$$

where $v_w^0 = 0.0307\ \mathrm{nm}^3$ denotes the simulated molecular volume of water in bulk at atmospheric pressure. The final production simulations are then performed in the (N_w, Π) ensemble at a pressure dictated by Eq. **2**, where the chemical potential is explicitly checked to satisfy the equality $\mu(N_w, \Pi) = \mu_0$ within an accuracy of $\Delta\mu = 0.01\ k_BT$, giving an error in the interaction pressure of $\Delta\Pi = \Delta\mu/v_w^0 = 1.5$ MPa or equivalently 15 atm. Further details on the TEM method are presented in the *SI Text*.

Molecular Dynamics Simulations. The simulation box contains 72 DPPC molecules ($N_l = 72$) forming a fluid lipid bilayer in water with 36 molecules per monolayer leaflet. DPPC is a zwitterionic phospholipid carrying no net charge. The membrane is arranged parallel to the (x, y)-plane without any position restraints and stabilized by the hydrophobic effect. The box dimensions in x and y directions are fixed and correspond to an average area per lipid of $A_l = 0.65\ \mathrm{nm}^2$, which is typical for PC lipids with saturated alkyl chains in the fluid L_α-phase (23). Periodic boundary conditions in all spatial directions are used. In this way a periodic stack of infinitely extended phospholipid membranes that interact across thin layers of water is atomistically represented. Simulations are performed at $T = 320$ K, above the chain melting temperature of DPPC membranes in experiment and previous MD studies employing the same lipid force field (20). The number of water molecules, N_w, is systematically varied to realize hydration degrees n_w ranging from 4 to 28 water molecules per lipid. For all simulations we use the GROMACS package (21) and SPC/E water (30) with SETTLE constraints (31) for the OH-bonds. We use the ffgmx force field in combination with a dedicated extension for lipid membrane simulations and the corresponding forcefield parameters for DPPC molecules (22, 32, 33). The simulation time step is $\Delta t = 2$ fs. Temperature is controlled using the Berendsen thermostat (34) with a time constant of $\tau_T = 0.1$ ps. In (N_w, Π, T, A) ensemble simulations (i.e., simulations with fixed N_w, T, A, and Π) we control the pressure in the z direction using the Berendsen barostat with anisotropic pressure coupling with a time constant of $\tau_p = 0.5$ ps and a compressibility parameter of $\kappa = 4.5 \times 10^{-10}\ \mathrm{Pa}^{-1}$. In ($N_w$, D, T, A) ensemble simulations the box height D is fixed instead. We use a plain LJ cut-off of 0.9 nm and account for electrostatic interactions using the particle-mesh-Ewald (PME) method (35, 36) with a 0.9 nm real-space cutoff. Prior to production runs the systems are equilibrated for 5 ns. Production runs have duration of at least 20 ns. For thermodynamic integration (see below) averages are taken over four independent parallel runs of 5 ns duration each.

Determination of the Chemical Potential. In thermal equilibrium the chemical potential of water, $\mu = \mu^{id} + \mu^{ex}$, is position independent. In a system with translational invariance (averaged over the simulation time) in x and y directions, the position-dependent ideal and excess parts, μ^{id} and μ^{ex}, only depend on z. In order to determine μ in the simulations, we measure $\mu^{id}(z) = k_BT \ln \rho(z)$ and $\mu^{ex}(z)$ at the z position chosen to be the center of the water layer. Here, $\rho(z)$ denotes the water density. The excess potential μ^{ex} is split into two parts that are determined independently, $\mu^{ex} = \mu_{LJ} + \mu_C$. μ_{LJ} denotes the excess chemical potential of a water molecule without partial charges (a rotationally symmetrical LJ particle in case of SPC/E), and is measured using the Widom test particle insertion (TPI) method (37, 38), in which the change in free energy upon the addition of a particle is quantified by monitoring the interactions of a randomly inserted particle with the molecules in an existing simulation trajectory. In order to measure $\mu_{LJ}(z)$, we use a modified GROMACS TPI code for particle insertion at selected z positions. μ_C

denotes the change in free energy upon addition of the partial charges of SPC/E water to the preinserted uncharged water molecule. This quantity is determined using the thermodynamic integration (TI) method (39), while keeping the water molecule at a selected z position using a harmonic restraint potential with a spring constant of $k = 50$ MJ/nm^2. TI relates the free energy difference between two states of a thermodynamic system to the averaged derivative $\langle \partial U(\lambda)/\partial\lambda \rangle$ of the potential energy $U(\lambda)$, where $\lambda = 0..1$ is a path variable. To obtain μ_C, the partial charges q_O and q_H belonging to the oxygen ("O") and hydrogen ("H") atoms of the water molecule are scaled linearly with the path variable, $q_m(\lambda) = \lambda Q_m$, where Q_m denotes the full partial charge, and $m \in \{O, H\}$. $\langle \partial U(\lambda)/\partial\lambda \rangle$ is evaluated for 21 equidistant λ values between 0 and 1. The resulting values are then fitted with a fifth order polynomial, and the fit is analytically integrated.

The chosen combination of TPI and TI allows for the precise determination of μ and thus for a high resolution in the interaction pressure. Typically, the simulation times are chosen such that the statistical errors $\delta\mu_{LJ}$ and $\delta\mu_C$ are both about 20 J/mol, determined from block averaging (for $\delta\mu_{LJ}$) or from the statistical distribution of results from independent parallel runs (for $\delta\mu_C$). The error in $\rho(z)$ is found to be negligible. The resulting statistical error in μ is then as low as $\delta\mu = \sqrt{\delta\mu_{LJ}^2 + \delta\mu_C^2} \approx 28$ J/mol $\approx 0.01\ k_B T$ and the corresponding error in the interaction pressure is $\delta\Pi = \delta\mu/v_w^0 \approx 1.5$ MPa. At small membrane separations, where interaction pressures are high, we are satisfied with larger error bars up to $\delta\mu \approx 0.4$ kJ/mol corresponding to $\delta\Pi \approx 20$ MPa. The reference chemical potential, $\mu_0 = (-28.44 \pm 0.01)$ kJ/mol, is averaged over a set of simulations with thick water layers ranging from 25 to 32 water molecules per lipid, where the interaction pressure is far below our detection limit and therefore negligible within the error. Further details on the simulation analysis are given in the supplement.

ACKNOWLEDGMENTS. Financial support from the Deutsche Forschungsgemeinschaft (DFG) within the Collaborative Research Center SFB 765 and the Ministry for Economy and Technology (BMWi) in an Allianz Industrie Forschung (AiF) project framework is gratefully acknowledged. The authors thank Dominik Horinek for insightful comments and the Leibniz Rechenzentrum München (LRZ) for computing time (project pr28xe).

1. Israelachvili JN, Wennerström H (1996) Role of hydration and water structure in biological and colloidal interactions. *Nature* 379:219–225.
2. LeNeveu DM, Rand RP, Parsegian VA (1976) Measurements of forces between lecithin bilayers. *Nature* 259:601–603.
3. Parsegian VA, Fuller N, Rand RP (1979) Measured work of deformation and repulsion of lecithin bilayers. *Proc Natl Acad Sci USA* 76:2750–2754.
4. Rand RP, Parsegian VA (1989) Hydration forces between phospholipid-bilayers. *Biochim Biophys Acta* 988:351–376.
5. Israelachvili JN, Adams GE (1978) Measurement of forces between two mica surfaces in aqueous electrolyte solutions in the range 0–100 nm. *J Chem Soc, Faraday Trans 1* 74:975–1001.
6. Marra J, Israelachvili JN (1985) Direct measurements of forces between phosphatidylcholine and phosphatidylethanolamine bilayers in aqueous electrolyte solutions. *Biochemistry* 24:4608–4618.
7. Parsegian VA, Zemb T (2011) Hydration forces: Observations, explanations, expectations, questions. *Curr Opin Colloid Interface Sci* 16:618–624.
8. Petrache HI, Zemb T, Belloni L, Parsegian VA (2006) Salt screening and specific ion adsorption determine neutral-lipid membrane interactions. *Proc Natl Acad Sci USA* 103:7982–7987.
9. Cevc G, Podgornik R, Zeks B (1982) The free energy, enthalpy, and entropy of hydration of phospholipid bilayer membranes and their dependence on the interfacial separation. *Chem Phys Lett* 91:193–196.
10. Israelachvili JN, Wennerström H (1992) Entropic forces between amphiphilic surfaces in liquids. *J Phys Chem* 96:520–531.
11. Marcelja S, Radic N (1976) Repulsion of interfaces due to boundary water. *Chem Phys Lett* 42:129–130.
12. Essmann U, Perera L, Berkowitz ML (1995) The Origin of the hydration interaction of lipid bilayers from MD simulation of dipalmitoylphosphatidylcholine membranes in gel and liquid crystalline phases. *Langmuir* 11:4519–4531.
13. Eun C, Berkowitz ML (2009) Origin of the hydration force: Water-mediated interaction between two hydrophilic plates. *J Phys Chem B* 113:13222–13228.
14. Eun C, Berkowitz ML (2010) Thermodynamic and hydrogen-bonding analyses of the interaction between model lipid bilayers. *J Phys Chem B* 114:3013–3019.
15. Hua L, Zangi R, Berne BJ (2009) Hydrophobic interactions and dewetting between plates with hydrophobic and hydrophilic domains. *J Phys Chem C* 113:5244–5253.
16. Pertsin A, Platonov D, Grunze M (2005) Direct computer simulation of water-mediated force between supported phospholipid membranes. *J Chem Phys* 122:244708.
17. Pertsin A, Platonov D, Grunze M (2007) Origin of short-range repulsion between hydrated phospholipid bilayers: A computer simulation study. *Langmuir* 23:1388–1393.
18. Raghavan K, Rami Reddy M, Berkowitz ML (1992) A molecular dynamics study of the structure and dynamics of water between dilauroylphosphatidylethanolamine bilayers. *Langmuir* 8:233–240.
19. Schneck E, Netz RR (2011) From simple surface models to lipid membranes: Universal aspects of the hydration interaction from solvent-explicit simulations. *Curr Opin Colloid Interface Sci* 16:607–611.
20. Schubert T, Schneck E, Tanaka M (2011) First order melting transitions of highly ordered DPPC gel phase membranes in molecular dynamics simulations with atomistic detail. *J Chem Phys* 135:055105.
21. Van der Spoel D, et al. (2005) GROMACS: Fast, flexible, and free. *J Comput Chem* 26:1701–1718.
22. Berger O, Edholm O, Jahnig F (1997) Molecular dynamics simulations of a fluid bilayer of dipalmitoylphosphatidylcholine at full hydration, constant pressure, and constant temperature. *Biophys J* 72:2002–2013.
23. Nagle JF, Tristram-Nagle S (2000) Structure of lipid bilayers. *Biochim Biophys Acta* 1469:159–195.
24. Israelachvili JN (1991) *Intermolecular and Surface Forces* (Academic, London).
25. Attard P, Mitchell DJ, Ninham BW (1988) The attractive forces between polar lipid bilayers. *Biophys J* 53:457–460.
26. Bonthuis DJ, Gekle S, Netz RR (2011) Dielectric profile of interfacial water and its effect on double-layer capacitance. *Phys Rev Lett* 107:166102.
27. Markova N, Sparr E, Wadsö L, Wennerström H (2000) A calorimetric study of phospholipid hydration. Simultaneous monitoring of enthalpy and free energy. *J Phys Chem B* 104:8053–8060.
28. Sparr E, Wennerström H (2011) Interlamellar forces and the thermodynamic characterization of lamellar phospholipid systems. *Curr Opin Colloid Interface Sci* 16:561–567.
29. Helfrich W (1978) Steric interaction of fluid membranes in multilayer systems. *Z Naturforsch* 33:305–315.
30. Berendsen HJC, Grigera JR, Straatsma TP (1987) The missing term in effective pair potentials. *J Phys Chem* 91:6269–6271.
31. Miyamoto S, Kollman PA (1992) SETTLE: An analytical version of the SHAKE and RATTLE algorithms for rigid water models. *J Comput Chem* 13:952–962.
32. Tieleman DP, Berendsen HJC (1996) Molecular dynamics simulations of a fully hydrated dipalmitoyl phosphatidylcholine bilayer with different macroscopic boundary conditions and parameters. *J Chem Phys* 105:4871–4880.
33. Tieleman DP, Marrink SJ, Berendsen HJC (1997) A computer perspective of membranes: Molecular dynamics studies of lipid bilayer systems. *Biochim Biophys Acta* 1331:235–270.
34. Berendsen HJC, Postma JPM, van Gunsteren WF, DiNola A, Haak JR (1984) Molecular dynamics with coupling to an external bath. *J Chem Phys* 81:3684–3690.
35. Darden T, York D, Pedersen L (1993) Particle mesh Ewald: An Nlog(N) method for Ewald sums in large systems. *J Chem Phys* 98:10089–10092.
36. Essmann U, et al. (1995) A smooth particle mesh Ewald method. *J Chem Phys* 103:8577–8593.
37. Binder K (1997) Applications of Monte Carlo methods to statistical physics. *Rep Prog Phys* 60:487–559.
38. Widom B (1963) Some topics in the theory of fluids. *J Chem Phys* 39:2808.
39. Frenkel D, Smit B (2002) *Understanding Molecular Simulation: From Algorithms to Applications* (Academic, San Diego, CA).

Supporting Information

Schneck et al. 10.1073/pnas.1205811109

SI Text

Online Supporting Material. ***Thermodynamic extrapolation.*** In the (N_w, D, T, A) ensemble, the chemical potential of water, $\mu(N_w, D, T, A)$, in general deviates from the bulk reference value $\mu_0(P, T)$. However, μ and the corresponding interaction pressure, $\Pi_{\mu\neq\mu_0}(N_w, T, A)$, can be used to determine the desired interaction pressure $\Pi_{\mu_0}(N_w, T, A)$ in the (N_w, μ_0, T, A) ensemble, abbreviated as $\Pi(N_w)$ in the main text, via extrapolation and depending on the deviation in the chemical potential:

$$\Pi_{\mu_0}(N_w, T, A) = \Pi_{\mu\neq\mu_0}(N_w, T, A) - \Delta\Pi(N_w, T, A, \mu_0, \mu). \quad [S1]$$

The correction term $\Delta\Pi$ can be written as a Taylor series in $\Delta\mu = \mu - \mu_0$ expanded around μ_0:

$$\Delta\Pi = \Delta\mu\left(\frac{\partial\Pi}{\partial\mu}\right)^{\mu=\mu_0}_{N_w,T,A} + \frac{(\Delta\mu)^2}{2}\left(\frac{\partial^2\Pi}{\partial\mu^2}\right)^{\mu=\mu_0}_{N_w,T,A} + \ldots \quad [S2]$$

We determine $(\partial\Pi/\partial\mu)_{N_w,T,A}$ in the following, starting from the the total differential of μ in the (N_w, D, T, A) ensemble:

$$d\mu(N_w, D, T, A) = \left(\frac{\partial\mu}{\partial N_w}\right)_{D,T,A} dN_w + \left(\frac{\partial\mu}{\partial T}\right)_{N_w,D,A} dT + \left(\frac{\partial\mu}{\partial D}\right)_{N_w,T,A} dD + \left(\frac{\partial\mu}{\partial A}\right)_{N_w,D,T} dA. \quad [S3]$$

Using the relation

$$dD(N_w, \Pi, T, A) = \left(\frac{\partial D}{\partial\Pi}\right)_{N_w,T,A} d\Pi + \left(\frac{\partial D}{\partial T}\right)_{N_w,\Pi,A} dT + \left(\frac{\partial D}{\partial N_w}\right)_{\Pi,T,A} dN_w + \left(\frac{\partial D}{\partial A}\right)_{N_w,\Pi,T} dA \quad [S4]$$

yields

$$\left(\frac{\partial\mu}{\partial\Pi}\right)_{N_w,T,A} = \left(\frac{\partial\mu}{\partial D}\right)_{N_w,T,A}\left(\frac{\partial D}{\partial\Pi}\right)_{N_w,T,A}, \quad [S5]$$

which can be rewritten as

$$\left(\frac{\partial\mu}{\partial\Pi}\right)_{N_w,T,A} = A\left(\frac{\partial\Pi}{\partial N_w}\right)_{D,T,A}\left(\frac{\partial N_w}{\partial\Pi}\right)_{D,T,A}\left(\frac{\partial D}{\partial N_w}\right)_{\Pi,T,A} = A\left(\frac{\partial D}{\partial N_w}\right)_{\Pi,T,A} \equiv v_w'(\Pi, T, A), \quad [S6]$$

where v_w' denotes the partial molecular volume of water between the surfaces at constant temperature, surface area, and interaction pressure. The first equality in Eq. **S6** follows from the Maxwell relation

$$\left(\frac{\partial\mu}{\partial D}\right)_{N_w,T,A} = \left(\frac{\partial}{\partial D}\left(\frac{\partial F}{\partial N_w}\right)_{D,T,A}\right)_{N_w,T,A} = \left(\frac{\partial}{\partial N_w}\left(\frac{\partial F}{\partial D}\right)_{N_w,T,A}\right)_{D,T,A} = -A\left(\frac{\partial\Pi}{\partial N_w}\right)_{D,T,A} \quad [S7]$$

and from the identity

$$\left(\frac{\partial D}{\partial\Pi}\right)_{N_w,T,A} = -\left(\frac{\partial N_w}{\partial\Pi}\right)_{D,T,A}\left(\frac{\partial D}{\partial N_w}\right)_{\Pi,T,A}, \quad [S8]$$

which is obtained from

$$dN_w(D, \Pi, T, A) = \left(\frac{\partial N_w}{\partial D}\right)_{\Pi,T,A} dD + \left(\frac{\partial N_w}{\partial\Pi}\right)_{D,T,A} d\Pi + \left(\frac{\partial N_w}{\partial T}\right)_{D,\Pi,A} dT + \left(\frac{\partial N_w}{\partial A}\right)_{D,\Pi,T} dA. \quad [S9]$$

Based on Eq. **S6**, Eq. **S2** can be rewritten as

$$\Delta\Pi = \frac{\Delta\mu}{v_w'} + \frac{(\Delta\mu)^2}{2}\left(\frac{\partial}{\partial\mu}\frac{1}{v_w'}\right)^{\mu=\mu_0}_{T,N_w,A} + \ldots \quad [S10]$$

Because water is almost incompressible up to the kilobar range (i.e., v_w' is approximately independent of μ), already the quadratic term in the expansion can be neglected to good approximation. We explicitly checked this in simulations, as shown in Fig. S1 for three hydration degrees ($n_w = 6$, 8, and 16) at $T = 320$ K. Red symbols correspond to (N_w, Π_{μ_0}, T, A) ensemble simulations, where $\mu = \mu_0$ (indicated with a horizontal dashed line) within the error. Solid lines represent approximations $d\mu/d\Pi = v_w^0$. As a consequence of the incompressible nature of water, v_w' is readily approximated as the partial molecular volume of water in bulk at constant pressure and temperature, v_w^0, which is determined independently,

$$v_w'(\Pi, T, A) \equiv A\left(\frac{\partial D}{\partial N_w}\right)_{\Pi,T,A} \approx \left(\frac{\partial V}{\partial N_w}\right)_{T,P} \equiv v_w^0. \quad [S11]$$

For extended simple point charge (SPC/E) water at 320 K and atmospheric pressure, we obtained $v_w^0 = 0.0307$ nm^3. Finally we are left with

$$\Pi_{\mu_0}(N_w, T, A) \approx \Pi_{\mu\neq\mu_0}(N_w, T, A) - \frac{\Delta\mu}{v_w^0}. \quad [S12]$$

Simulation analysis. The interaction pressure Π_{μ_0} is determined using thermodynamic extrapolation (see above). Its indirect contribution, Π_{ind}, defined as the normal force per unit area exerted on each lipid monolayer by the water layer, is determined by summing over the atomic lipid/water pair forces in (N_w, Π_{μ_0}, T, A) ensemble simulations (i.e., simulations with fixed N_w, T, A, and $\Pi = \Pi_{\mu_0}$). The direct contribution, Π_{dir}, defined as the normal force per unit area exerted on each lipid monolayer by the proximal monolayer of the opposing lipid bilayer, is then calculated as $\Pi_{\text{dir}} = \Pi_{\mu_0} - \Pi_{\text{ind}}$. Direct ($G_{\text{dir}}$) and indirect ($G_{\text{ind}}$) contributions to the interaction free energy $G = G_{\text{dir}} + G_{\text{ind}}$ are calculated by integrating Π_{dir} and Π_{ind}, respectively, along D_w:

$$G_{\text{dir}}(D_w) = \int_{D_w}^{\infty} \Pi_{\text{dir}}(D_w')dD_w', \quad [S13]$$

$$G_{\mathrm{ind}}(D_w) = \int_{D_w}^{\infty} \Pi_{\mathrm{ind}}(D_w')dD_w'. \quad \textbf{[S14]}$$

Enthalpies are approximated by system internal energies, because the work of expansion due to variations in total system volume (including the volume of water transferred into bulk) upon dehydration is negligible [$P\Delta V/A \ll 0.1$ kJ/(mol nm^2)]. The enthalpy of the total interaction, H, is determined by measuring the system energy in (N_w, Π_{μ_0}, T, A) ensemble simulations, while taking into account the enthalpy contribution ΔH_w of water molecules transferred from the region between the membranes into the surrounding bulk upon dehydration:

$$\Delta H_w = \Delta N_w \left(\frac{dH}{dN_w}\right)_{P,T}^{\mathrm{bulk}}, \quad \textbf{[S15]}$$

where ΔN_w is the number of transferred water molecules and $(dH/dN_w)_{P,T}^{\mathrm{bulk}}$ is determined as −45.15 kJ/mol in independent bulk water simulations. For the comparison with calorimetry experiments under atmospheric pressure (1), we subtract the contribution ΔH_{int} originating from the internal compression of the membranes upon pressure exertion in the (N_w, Π_{μ_0}, T, A) ensemble simulations. ΔH_{int} is approximated linearly, $\Delta H_{\mathrm{int}} = \alpha\Pi$ (see Fig. S2), where $\alpha = dH_{\mathrm{int}}/d\Pi = (-0.25 \pm 0.06)$ kJ/(mol bar), as determined independently from the lipid–lipid interaction energies in simulations of a highly hydrated membrane ($n_w = 28$) at various pressures. Error bars in Fig. 2 of the main text account for the error in ΔH_{int}. The enthalpy of the direct interaction, H_{dir}, is determined by measuring all lipid–lipid interaction energies in the simulation trajectories. ΔH_{int} is again subtracted for consistency. The enthalpy of the indirect interaction, H_{ind}, is then determined as $H_{\mathrm{ind}} = H - H_{\mathrm{dir}}$.

The entropic terms of direct, indirect, and total interaction are calculated as

$$-TS_{\mathrm{dir}} = G_{\mathrm{dir}} - H_{\mathrm{dir}}, \quad \textbf{[S16]}$$

$$-TS_{\mathrm{ind}} = G_{\mathrm{ind}} - H_{\mathrm{ind}}, \quad \textbf{[S17]}$$

$$-TS = G - H. \quad \textbf{[S18]}$$

Water excess enthalpy profiles, $h_{\mathrm{ind}}(z)$, are calculated from Lennard–Jones (LJ) and short-range Coulomb pair-interactions averaged over 100 probe water molecules. We confirmed that taking into account long-range electrostatic interactions (as implemented in the particle-mesh Ewald (PME) method) does not alter the profiles significantly.

Definition of the water layer thickness. The thickness D_w of the water layer was defined according to the classical experimental studies of Parsegian, Rand, and coworkers (2), based on the volume v_w occupied by a water molecule:

$$D_w = \frac{2n_w v_w}{A_l}, \quad \textbf{[S19]}$$

where $A_l = 2A/N_l$ denotes the membrane area per phospholipid molecule and $n_w = N_w/N_l$ the number of water molecules apportioned to one phospholipid molecule at a given hydration degree. We account for the pressure dependence of v_w, approximated with the linear expression

$$v_w(\Pi) = v_w^0 + \Pi\frac{dv_w}{d\Pi}, \quad \textbf{[S20]}$$

where $v_w^0 = 0.0307$ nm^3 and $dv_w/d\Pi \approx dv_w/dP = -1.44 \times 10^{-11}$ nm^3/Pa, as determined in independent bulk water simulations (see Fig. S3 showing the volume per water molecule v_w as a function of the pressure together with a linear fit). This corresponds to a compressibility of $\kappa = -(1/v_w^0)(dv_w/dP) = 4.7 \times 10^{-10}$ Pa^{-1}, close to the experimental value 4.4×10^{-10} Pa^{-1} (3).

LJ and coulomb contributions to the indirect interaction enthalpy. Fig. S4 shows a decomposition of the indirect interaction enthalpy, H_{ind}, into its Coulomb and LJ contributions. It is seen that H_{ind} is dominated by the Coulomb part.

Polarization profile in a Ginzburg–Landau treatment. As introduced by Marcelja and Radic for a general polar order parameter (4), the free energy density $g(z)$ connected to the mean polarization $p(z) = \langle cos\theta(z)\rangle$ can be expressed as

$$g(z) = ap^2(z) + c(dp(z)/dz)^2, \quad \textbf{[S21]}$$

where θ denotes the angle between the water dipole vector and the surface normal, and a and c are unspecified prefactors. The free energy in the interval $[-D'/2, D'/2]$ then follows as

$$G(D') = \int_{-D'/2}^{D'/2} g(z)dz. \quad \textbf{[S22]}$$

G becomes minimal when p satisfies the differential equation

$$ap - c\frac{d^2p}{dz^2} = 0. \quad \textbf{[S23]}$$

In the antisymmetrical case of oppositely polarizing surfaces, where $p(-D'/2) = -p(D'/2) = p_0$, Eq. **S23** has the solution

$$p(z) = p_0\frac{\sinh(z/\lambda)}{\sinh(D'/(2\lambda))}, \quad \textbf{[S24]}$$

with $\lambda = \sqrt{c/a}$. The solid lines in Fig. 4*C* in the main text correspond to simultaneous fits of this expression to the polarization profiles in the interval $[-D'/2, D'/2]$ with free parameters p_0 and λ. Here, $D' = D_w - \Delta D$, where $\Delta D = 1.0$ nm was chosen such that the water density does not fall below 90% of the bulk value in the fit interval.

1. Markova N, Sparr E, Wadsö L, Wennerström H, (2000) A calorimetric study of phospholipid hydration. simultaneous monitoring of enthalpy and free energy. *J Phys Chem B* 104:8053–8060.
2. Parsegian VA, Fuller N, Rand RP, (1979) Measured work of deformation and repulsion of lecithin bilayers. *Proc Natl Acad Sci USA* 76:2750–2754.
3. Fine RA, Millero FJ, (1973) Compressibility of water as a function of temperature and pressure. *J Chem Phys* 59:5529–5536.
4. Marcelja S, Radic N, (1976) Repulsion of interfaces due to boundary water. *Chem Phys Lett* 42:129–130.

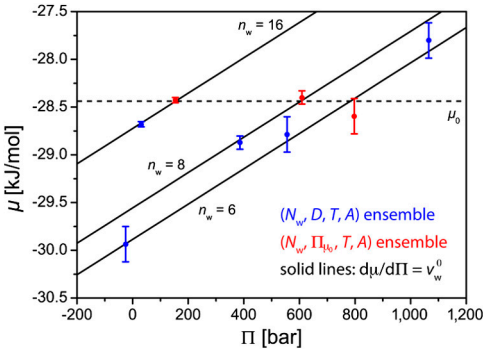

Fig. S1. Chemical potential of water between phospholipid membranes as a function of the pressure at various degrees of hydration ($n_w = 6$, 8, and 16) at $T = 320$ K (symbols). Red symbols correspond to (N_w, Π_{μ_0}, T, A) ensemble simulations, where $\mu = \mu_0$ (indicated with a horizontal dashed line) within the error. Solid lines: Approximation $d\mu/d\Pi = v_w^0$.

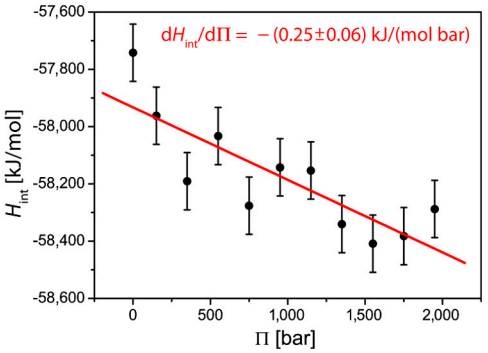

Fig. S2. Enthalpy of membrane internal compression H_{int} as a function of the pressure (symbols) and linear fit (solid red line). Data points are lipid–lipid interaction energies determined in simulations of a highly hydrated membrane subject to various pressures.

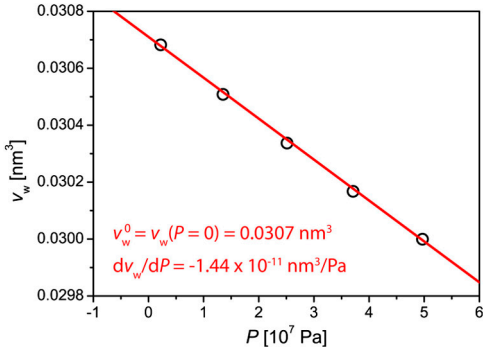

Fig. S3. Volume per water molecule v_w as a function of the pressure in bulk water simulations (symbols) and linear fit (solid red line).

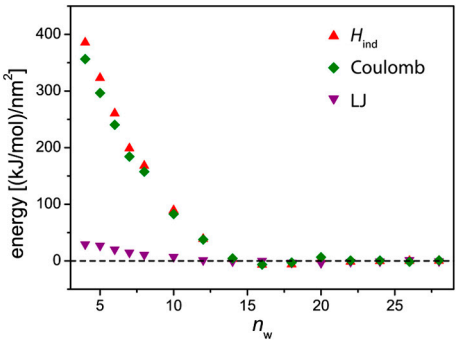

Fig. S4. Coulomb and LJ contributions to the indirect interaction enthalpy, H_{ind}, as a function of n_w.